

Constraints on the momentum dependence of nuclear symmetry potential from Sn + Sn collisions at 270 MeV/nucleon

Gao-Feng Wei,^{1,2,*} Xin Huang,¹ Qi-Jun Zhi,^{1,2} Ai-Jun Dong,^{1,2} Chang-Gen Peng,³ and Zheng-Wen Long⁴

¹*School of Physics and Electronic Science, Guizhou Normal University, Guiyang 550025, China*

²*Guizhou Provincial Key Laboratory of Radio Astronomy and Data Processing,
Guizhou Normal University, Guiyang 550025, China*

³*Guizhou Provincial Key Laboratory of Public Big Data, Guizhou University, Guiyang 550025, China*

⁴*College of Physics, Guizhou University, Guiyang 550025, China*

Within a transport model, we employ the central Sn + Sn collisions at 270 MeV/nucleon to constrain the momentum dependence of nuclear symmetry potential that can be characterised by the value of nuclear symmetry potential at the saturation density and infinitely large nucleon momentum, i.e., $U_{sym}^{\infty}(\rho_0)$. Through comparing the charged pion yields as well as their single and double pion ratios of the theoretical simulations for the reactions $^{108}\text{Sn} + ^{112}\text{Sn}$ and $^{132}\text{Sn} + ^{124}\text{Sn}$ with the corresponding data in S π RIT experiments, as well as conducting the systematic error analyses, the value of $U_{sym}^{\infty}(\rho_0)$ can be constrained into a certain range that ensures the errors between theoretical simulations of pion observables and corresponding data in S π RIT experiments to be within 4%. Moreover, the related isospin splitting of in-medium nucleon effective mass is also discussed within the constrained $U_{sym}^{\infty}(\rho_0)$.

I. INTRODUCTION

The equation of state (EoS) of asymmetric nuclear matter (ANM) especially its nuclear symmetry energy term plays an essential role in studying the structure and evolution of radioactive nuclei as well as the synthesis of medium and heavy nuclei [1–9]. The nuclear symmetry energy characterizes the variation of EoS of the symmetric nuclear matter (SNM) to that of the pure neutron matter (PNM), the latter is closely connected to the neutron star (NS) matter. Naturally, the properties of NS such as the radius as well as the deformation of NS merger are also closely related to the nuclear symmetry energy especially that at densities of about twice the saturation density ρ_0 [10–17]. Nevertheless, knowledge on the nuclear symmetry energy at suprasaturation densities is still far from satisfactory so far, although that around and below ρ_0 [18] as well as the isospin-independent part of EoS for ANM, i.e., EoS of SNM [19, 20], are relatively well determined. Essentially, the EoS of ANM and its nuclear symmetry energy term are determined by the nuclear mean field especially its isovector part, i.e., the nuclear symmetry potential. However, because of the extreme challenge of relatively direct detection of nuclear symmetry potential in experiments, one only extracted using the nucleon-nucleus scattering and (p,n) charge-exchange reactions between isobaric analog states limited information of nuclear symmetry potential at ρ_0 , and parameterized as $U_{sym}(\rho_0, E_k) = a - bE_k$, where $a \approx 22 - 34$ MeV, $b \approx 0.1 - 0.2$ and E_k is limited to no more than 200 MeV [21–23].

Heavy-ion collision (HIC) using some isospin-sensitive observables is one of the most promising approaches to explore the nuclear symmetry potential/energy especially

at suprasaturation densities [3, 4, 10, 24–26]. Very recently, the S π RIT collaboration reported the results from the first measurement dedicated to probe the nuclear symmetry energy at suprasaturation densities via pion production in Sn + Sn collisions at 270 MeV/nucleon carried out at RIKEN-RIBF in Japan [24]. Moreover, they compared the charged pion yields as well as their single and double pion ratios with the corresponding simulation results from seven transport models. Qualitatively, the theoretical simulations from seven transport models reach an agreement with the data, yet quantitatively, almost all the models cannot very satisfactorily reproduce both the pion yields and their single as well as double pion ratios of the experimental data [24]. To this situation, author in Ref. [27] claimed that through considering about 20% high momentum nucleons in colliding nuclei can reproduce quite well both the charged pion yields and their pion ratios of the experimental data, due to the fact that high momentum distribution in nuclei caused by the short-range correlations (SRCs) has been strongly demonstrated both in experiments and theories [28–33]. Following this work, we focus on the momentum dependence of nuclear symmetry potential since that plays a more important role in probing the high density nuclear symmetry energy [34–37]. Actually, as indicated in Ref. [24], the possible reasons for the unsatisfactory of seven models quantitatively fitting experimental data may be different assumptions regarding the mean field potential, pion potential as well as the treatment of Coulomb field. Therefore, it is very necessary to explore how the momentum dependence of nuclear symmetry potential affects the pion production in HICs. As to other factors indicated in Ref. [24], we also give detailed consideration according to some sophisticated treatment ways as discussed in model description.

* E-mail: wei.gaofeng@gznu.edu.cn

II. THE MODEL

This study is carried out within an isospin- and momentum-dependent Boltzmann-Uehling-Uhlenbeck (IBUU) transport model. In the framework, the present version of IBUU model originates from the IBUU04 [38, 39] and/or IBUU11 [40] models. However, the present version of IBUU model has been greatly improved to achieve more accurate simulations of the pion production as discussed in the following.

First, a separate density-dependent scenario for the in-medium nucleon-nucleon interaction [41–43], i.e.,

$$v_D = t_0(1 + x_0 P_\sigma)[\rho_{\tau_i}(\mathbf{r}_i) + \rho_{\tau_j}(\mathbf{r}_j)]^\alpha \delta(\mathbf{r}_{ij}), \quad (1)$$

is used to replace the density-dependent term of original Gogny effective interaction [44], i.e.,

$$v(r) = \sum_{i=1,2} (W + B P_\sigma - H P_\tau - M P_\sigma P_\tau)_i e^{-r^2/\mu_i^2} + t_0(1 + x_0 P_\sigma) \left[\rho \left(\frac{\mathbf{r}_i + \mathbf{r}_j}{2} \right) \right]^\alpha \delta(\mathbf{r}_{ij}), \quad (2)$$

where W , B , H , M , and μ are five parameters, P_τ and P_σ are the isospin and spin exchange operators, respectively; while α is the density dependent parameter used to mimic in-medium effects of the many-body interactions [41–43]. Correspondingly, the potential energy density for ANM with this improved momentum-dependent interaction (IMDI) is expressed [42] as

$$V(\rho, \delta) = \frac{A_u(x)\rho_n\rho_p}{\rho_0} + \frac{A_l(x)}{2\rho_0}(\rho_n^2 + \rho_p^2) + \frac{B}{\sigma+1} \frac{\rho^{\sigma+1}}{\rho_0^\sigma} \times \left\{ \frac{1+x}{2}(1-\delta)^2 + \frac{1-x}{4} [(1+\delta)^{\sigma+1} + (1-\delta)^{\sigma+1}] \right\} + \frac{1}{\rho_0} \sum_{\tau, \tau'} C_{\tau, \tau'} \int \int d^3p d^3p' \frac{f_\tau(\vec{r}, \vec{p}) f_{\tau'}(\vec{r}, \vec{p}')}{1 + (\vec{p} - \vec{p}')^2/\Lambda^2}. \quad (3)$$

In the mean-field approximation, Eq. (3) leads to the following single-nucleon potential for the present IBUU model [41–43],

$$U(\rho, \delta, \vec{p}, \tau) = A_u(x) \frac{\rho_{-\tau}}{\rho_0} + A_l(x) \frac{\rho_\tau}{\rho_0} + \frac{B}{2} \left(\frac{2\rho_\tau}{\rho_0} \right)^\sigma (1-x) + \frac{2B}{\sigma+1} \left(\frac{\rho}{\rho_0} \right)^\sigma (1+x) \frac{\rho_{-\tau}}{\rho} \left[1 + (\sigma-1) \frac{\rho_\tau}{\rho} \right] + \frac{2C_l}{\rho_0} \int d^3p' \frac{f_\tau(\vec{p}')}{1 + (\vec{p} - \vec{p}')^2/\Lambda^2} + \frac{2C_u}{\rho_0} \int d^3p' \frac{f_{-\tau}(\vec{p}')}{1 + (\vec{p} - \vec{p}')^2/\Lambda^2}, \quad (4)$$

where $\sigma = \alpha + 1$, $\tau = 1$ for neutrons and -1 for protons, and the parameters $A_u(x)$, $A_l(x)$, $C_u(\equiv C_{\tau, -\tau})$ and $C_l(\equiv$

$C_{\tau, \tau})$ are expressed as

$$A_l(x) = A_{l0} + U_{sym}^\infty(\rho_0) - \frac{2B}{\sigma+1} \times \left[\frac{(1-x)}{4} \sigma(\sigma+1) - \frac{1+x}{2} \right], \quad (5)$$

$$A_u(x) = A_{u0} - U_{sym}^\infty(\rho_0) + \frac{2B}{\sigma+1} \times \left[\frac{(1-x)}{4} \sigma(\sigma+1) - \frac{1+x}{2} \right], \quad (6)$$

$$C_l = C_{l0} - 2U_{sym}^\infty(\rho_0) \frac{p_{f0}^2}{\Lambda^2 \ln [(4p_{f0}^2 + \Lambda^2)/\Lambda^2]}, \quad (7)$$

$$C_u = C_{u0} + 2U_{sym}^\infty(\rho_0) \frac{p_{f0}^2}{\Lambda^2 \ln [(4p_{f0}^2 + \Lambda^2)/\Lambda^2]}, \quad (8)$$

where p_{f0} is the nucleon Fermi momentum in SNM at ρ_0 , and $U_{sym}^\infty(\rho_0)$ is used to characterize the momentum dependence of nuclear symmetry potential at ρ_0 . Presently, knowledge on the momentum dependence of nuclear symmetry potential even at ρ_0 is rather limited as aforementioned [21–23]. Therefore, taking the current consensus on the momentum dependence of nuclear symmetry potential as a reference, we treat the $U_{sym}^\infty(\rho_0)$ as a free parameter similar as the x parameter, that is used to mimic the slope value $L \equiv 3\rho(dE_{sym}/d\rho)$ of nuclear symmetry energy at ρ_0 without changing the value of nuclear symmetry energy $E_{sym}(\rho)$ at ρ_0 and any properties of the SNM. Actually, a similar quantity (i.e., y parameter) in Refs. [45, 46] has been used to describe the momentum dependence of nuclear symmetry potential at ρ_0 , however, the quantitative constraints on it are not concluded. In addition, it should be mentioned that the B -terms in Eqs. (3) and (4) as well as in the expressions of A_u and A_l are completely different from that in Refs. [45, 46]. This is exactly because the separate density-dependent scenario for in-medium nucleon-nucleon interaction has been adopted in the present model to more delicate treatment of the in-medium many-body force effects [42] that also affects significantly the pion production in HICs [43]. The parameters A_{l0} , A_{u0} , B , σ , C_{l0} , C_{u0} and Λ are determined by fitting experimental and/or empirical constraints on properties of nuclear matter at $\rho_0 = 0.16 \text{ fm}^{-3}$, i.e., the binding energy -16 MeV , the incompressibility $K_0 = 230 \text{ MeV}$ for SNM, the isoscalar effective mass $m_s^* = 0.7m$, the isoscalar potential at infinitely large nucleon momentum $U_0^\infty(\rho_0) = 75 \text{ MeV}$, as well as the nuclear symmetry energy $E_{sym}(\rho_0) = 32.5 \text{ MeV}$. The values of these parameters are $A_{l0} = A_{u0} = -66.963 \text{ MeV}$, $B = 141.963 \text{ MeV}$, $C_{l0} = -60.486 \text{ MeV}$, $C_{u0} = -99.702 \text{ MeV}$, $\sigma = 1.2652$, and $\Lambda = 2.424p_{f0}$.

Shown in Fig. 1 is the kinetic-energy dependent isoscalar potential at ρ_0 calculated from the IMDI interaction in comparison with the Schrödinger-equivalent isoscalar potential obtained by Hama *et al.* [47, 48]. Obviously, quite good consistency can be seen for the isoscalar potential between the present model and that of the

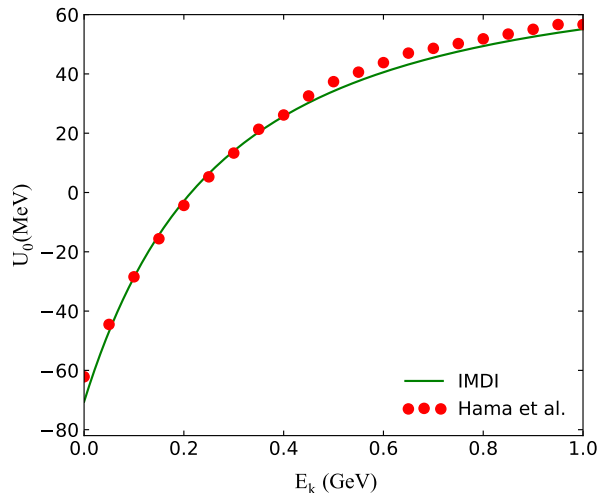


FIG. 1. (Color online) Kinetic-energy dependent isoscalar potentials at ρ_0 calculated from the IMDI interaction in comparison with the Schrödinger-equivalent isoscalar potential obtained by Hama *et al.*

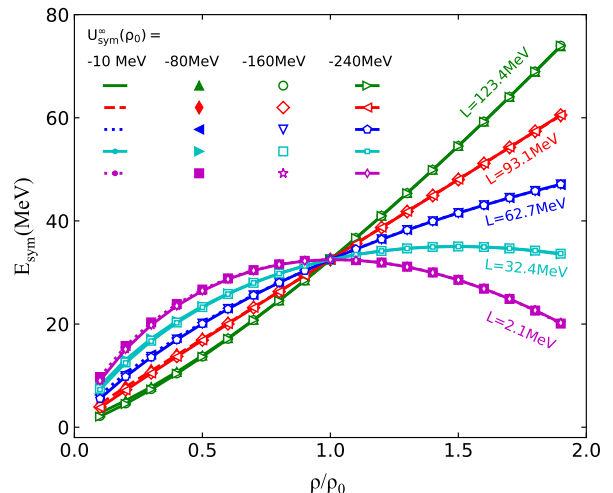


FIG. 3. (Color online) Density dependence of the nuclear symmetry energy with different $U_{sym}^\infty(\rho_0)$ calculated from the IMDI interaction.

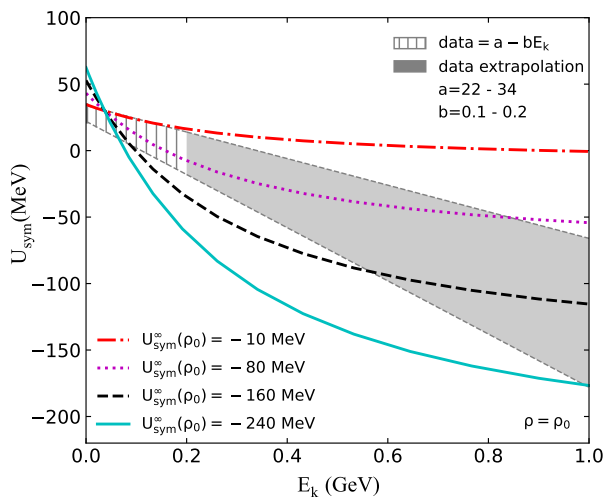


FIG. 2. (Color online) Momentum/kinetic-energy dependent nuclear symmetry potential at ρ_0 with different $U_{sym}^\infty(\rho_0)$ calculated from the IMDI interaction and the parameterized one from the experimental and/or empirical data.

Hama *et al.* Shown in Fig. 2 are the momentum/kinetic-energy dependent nuclear symmetry potential at ρ_0 with different $U_{sym}^\infty(\rho_0)$ calculated from the IMDI interaction and the parameterized one from the experimental and/or empirical data [21–23]. To provide more intuitive references for the $U_{sym}^\infty(\rho_0)$, we also extrapolate the experimental and/or empirical nuclear symmetry potential to nucleon kinetic energy up to 1 GeV. It is seen that the values of our nuclear symmetry potentials at Fermi kinetic energy (i.e., about 36.8 MeV) even with different $U_{sym}^\infty(\rho_0)$ are the same and also within the allowed range of experimental and/or empirical data. Actually, it is ex-

actly based on the values of nuclear symmetry potentials at the Fermi kinetic energy and the infinitely nucleon momentum that we determine the momentum dependence of nuclear symmetry potential at ρ_0 . On the other hand, since the isoscalar potentials are unchanged with different $U_{sym}^\infty(\rho_0)$, one naturally expects the differences of momentum dependence between nuclear symmetry potentials with different $U_{sym}^\infty(\rho_0)$ can be reflected by the pion observable in HICs, because the different nuclear symmetry potential can lead to the different isospin effects and thus different π^-/π^+ ratios for neutron-rich reactions. Nevertheless, to get the pion observable more cleanly reflecting effects of the momentum dependence of nuclear symmetry potential, the effects of high density symmetry energy (i.e., L that is controlled by the x parameter) on the pion observable should be isolated. To this end, it is useful to map the momentum dependent nuclear symmetry potentials with different $U_{sym}^\infty(\rho_0)$ into cases that have the same nuclear symmetry energy. This is carried out by fitting the identical constraints for SNM as well as the identical slope parameter of nuclear symmetry energy at ρ_0 , the corresponding results are also shown in Fig. 3. It is seen that even with the same nuclear symmetry energy, the corresponding nuclear symmetry potential could be very different since the fact that the nuclear symmetry potentials depend not only on the nucleon density but also on the nucleon momentum or energy.

Second, to more accurate simulations of pion production in HICs, we also consider the Δ potential and pion potential effects in HICs. For the Δ potential, instead of using the usual ansatz of setting the Δ potential equal to that of nucleons, we adjust the depth of Δ potential by a factor 2/3 to that of nucleons due to the fact that the depth of nucleon potential is approximately -50 MeV while that of the Δ potential is empirically constrained

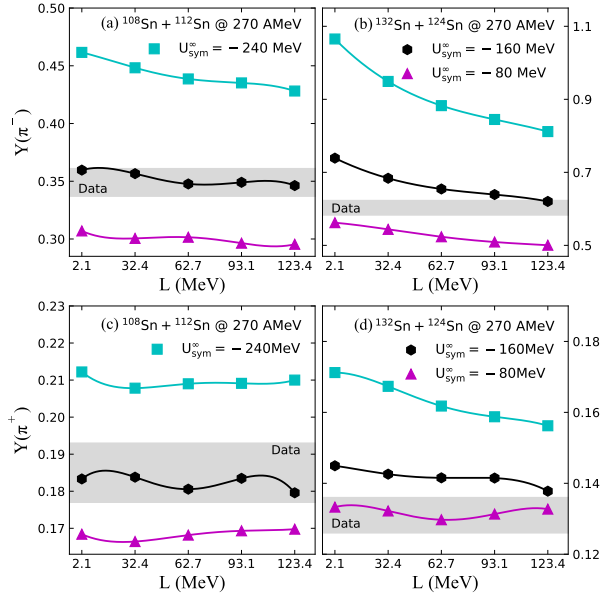


FIG. 4. (Color online) Upper: Multiplicities of π^- generated in reactions $^{108}\text{Sn} + ^{112}\text{Sn}$ (a) and $^{132}\text{Sn} + ^{124}\text{Sn}$ (b) with different $U_{sym}^\infty(\rho_0)$ as a function of the L in comparison with the corresponding S π RIT data; Lower: Multiplicities of π^+ generated in reactions $^{108}\text{Sn} + ^{112}\text{Sn}$ (c) and $^{132}\text{Sn} + ^{124}\text{Sn}$ (d) with different $U_{sym}^\infty(\rho_0)$ as a function of the L in comparison with the corresponding S π RIT data.

around -30 MeV [48–51], for the specific expression of the Δ potential, see Ref. [52] for the details. Pion potential is another factor that also might affect the pion production in HICs as indicated in Refs. [10, 24, 53–56]. Therefore, we also consider the pion potential effects in this study. Specifically, when the pionic momentum is higher than 140 MeV/ c , we use the pion potential based on the Δ -hole model, of the form adopted in Ref. [48]; when the pionic momentum is lower than 80 MeV/ c , we adopt the pion potential of the form used in Refs. [49–51]; while for the pionic momentum falling into the range from 80 to 140 MeV/ c , an interpolative pion potential constructed in Ref. [48] is used. It should be mentioned that the present pion potential includes the isospin- and momentum-dependent pion s -wave and p -wave potentials in nuclear medium as that in Ref. [56], see Refs. [48–51] for the details.

Finally, as to the treatment of Coulomb field as indicated in Refs. [10, 24], we calculate the electromagnetic (EM) interactions from the Maxwell equation, i.e., $\mathbf{E} = -\nabla\varphi - \partial\mathbf{A}/\partial t$, $\mathbf{B} = \nabla \times \mathbf{A}$, where the scalar potential φ and vector potential \mathbf{A} of EM fields are calculated from the resources of charges Ze and currents $Ze\mathbf{v}$. For the detailed EM field effects in HICs, we refer readers to Refs. [52, 57, 58] for more details.

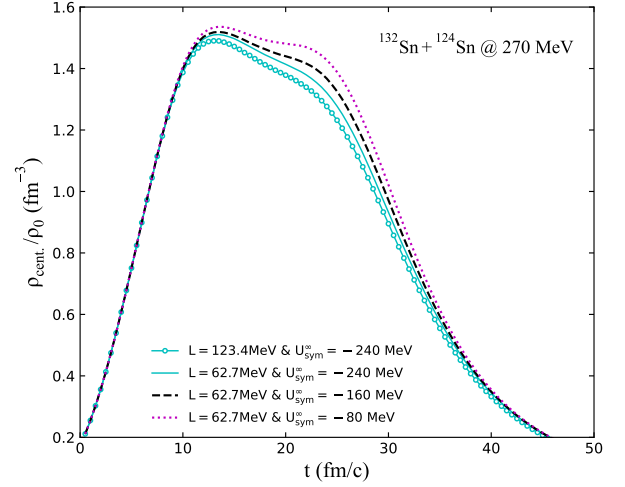


FIG. 5. (Color online) Evolution of the reduced average densities in central region ($\rho_{\text{cent.}}/\rho_0$) produced in $^{132}\text{Sn} + ^{124}\text{Sn}$ reactions at 270 MeV/nucleon.

III. RESULTS AND DISCUSSIONS

Now, we turn to the pion production in $^{108}\text{Sn} + ^{112}\text{Sn}$ and $^{132}\text{Sn} + ^{124}\text{Sn}$ reactions at 270 MeV/nucleon with an impact parameter of $b = 3$ fm. To study the sensitivities of pion yields on the high density symmetry energy (i.e., L) and the momentum dependence of nuclear symmetry potential (i.e., $U_{sym}^\infty(\rho_0)$), pion yields as a function of the L for different $U_{sym}^\infty(\rho_0)$ settings in the reactions are shown in Fig. 4. First, consistent with the findings in Refs. [27, 59], it is seen that the multiplicities of π^- are more sensitive to the L compared to those of π^+ , in particular for the larger isospin asymmetry reactions $^{132}\text{Sn} + ^{124}\text{Sn}$, since the π^- is mostly produced from the neutron-neutron inelastic collisions [59]. Second, it is seen that with a certain L value the nuclear symmetry potential with larger value of $|U_{sym}^\infty(\rho_0)|$ leads to more production of π^- and π^+ . To understand this observation, we first check the evolution of central region densities formed in HICs. Shown in Fig. 5 are the evolutions of central reduced densities $\rho_{\text{cent.}}/\rho_0$ formed in $^{132}\text{Sn} + ^{124}\text{Sn}$ reactions with different $U_{sym}^\infty(\rho_0)$ but a certain L of 62.7 MeV. For comparison, we also show the evolution of $\rho_{\text{cent.}}/\rho_0$ for the same reaction with the $L = 123.4$ MeV and $U_{sym}^\infty(\rho_0) = -240$ MeV. It is seen that with a certain $U_{sym}^\infty(\rho_0) = -240$ MeV the soft symmetry energy with $L = 62.7$ MeV leads to a higher compression compared to that with a stiff symmetry energy $L = 123.4$ MeV in agreement with previous observations in many studies. Interestingly, we notice that with a certain $L = 62.7$ MeV the $U_{sym}^\infty(\rho_0)$ also affects the evolution of central region densities. Specifically, approximately at 13 fm/ c independent of $U_{sym}^\infty(\rho_0)$, the reaction with a certain $L = 62.7$ MeV approaches maximum compression and thus generates a maximum compression

densities $1.5\rho_0$ in the central region, however, the decreasing velocity of this density is a little faster in case with more larger $|U_{sym}^\infty(\rho_0)|$. This is due to the nuclear symmetry potential with more larger $|U_{sym}^\infty(\rho_0)|$ causes some high density nucleons to gain more acceleration in the subsequent reaction stages, and thus leading to the densities of compression region to reduce slightly faster. This can be demonstrated by checking the kinetic energy distribution of nucleons in compression region with local densities higher than ρ_0 at $t = 20$ fm/c as shown in Fig. 6. Obviously, with a certain $L = 62.7$ MeV but varying the $U_{sym}^\infty(\rho_0)$ from -80 to -240 MeV, we indeed can observe increased high energy nucleons but reduced low energy nucleons. In general, since the scalar potential has the same repulsive effects on neutrons and protons, while the nuclear symmetry potential has the repulsive (attractive) effects on the high density but low energy¹ neutrons (protons), it is natural that one might expect these high energy nucleons to be neutrons. Nevertheless, as shown in Fig. 7, these high energy nucleons contain both neutrons and protons, and of course, neutrons outnumber protons due to the reaction itself is neutron-rich system. Moreover, as indicated by the arrow in Fig. 6, the kinetic energies of these energetic neutrons and protons are above 150 MeV, while the threshold energy of pion production through NN inelastic collisions is lower than 300 MeV; Naturally, with a certain L but varying the $U_{sym}^\infty(\rho_0)$ from -80 to -240 MeV, we can understand the increased production of both π^- and π^+ shown in Fig. 4 since the π^- and π^+ are produced mainly from inelastic $nn \rightarrow p\pi^-$ and $pp \rightarrow n\pi^+$ channels. Third, compared with the S π RIT data as shown in Fig. 4, our results on both π^- and π^+ yields with a certain range of $U_{sym}^\infty(\rho_0)$ indeed can fit the experimental pion data. This finding naturally provides the opportunity to constrain the value of $U_{sym}^\infty(\rho_0)$ through comparing the pion yields of theoretical simulations with the corresponding data.

So far, one might wonder the nuclear symmetry potential at $1.5\rho_0$ (i.e., attainable maximum densities in the compressed stage) with a certain L but varying $U_{sym}^\infty(\rho_0)$ from -80 to -240 MeV could cause both high energy neutrons and protons to increase. In order to understand this observation, we show in right panel of Fig. 8 the nuclear symmetry potential at $1.5\rho_0$ with a certain $L = 62.7$ MeV but different $U_{sym}^\infty(\rho_0)$. For completeness, we also show in left panel of Fig. 8 the corresponding nuclear symmetry potential at low densities (i.e., $0.5\rho_0$). It is seen that similar to the nuclear symmetry potential at ρ_0 , the nuclear symmetry potentials at $1.5\rho_0$ even with different $U_{sym}^\infty(\rho_0)$ have a same value approximately at the nucleon kinetic energy of 47 MeV. In addition, the value of nuclear symmetry potential also

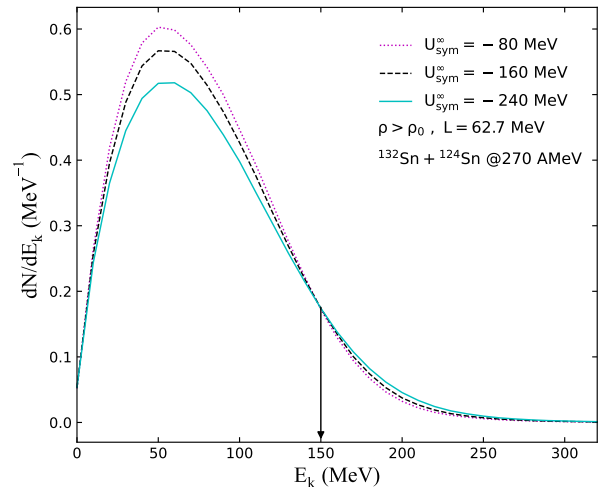


FIG. 6. (Color online) Kinetic-energy distribution of nucleons in compression region at $t = 20$ fm/c in $^{132}\text{Sn} + ^{124}\text{Sn}$ reactions at 270 MeV/nucleon.

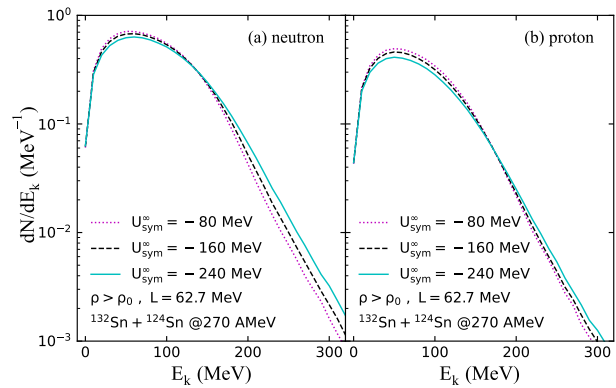


FIG. 7. (Color online) Kinetic-energy distribution of neutrons (a) and protons (b) in compression region at $t = 20$ fm/c in $^{132}\text{Sn} + ^{124}\text{Sn}$ reactions at 270 MeV/nucleon.

changes from positive to negative when the kinetic energy of nucleon is larger than a certain value depending on the value of $U_{sym}^\infty(\rho_0)$. Specifically, with a certain $L = 62.7$ MeV but varying the $U_{sym}^\infty(\rho_0)$ from -80 to -240 MeV, protons (neutrons) in high density phase will feel more stronger attractive (repulsive) effects from nuclear symmetry potentials when their kinetic energies are lower than 47 MeV; In contrast, if their kinetic energies are larger than 47 MeV but lower than about 81 MeV,² protons (neutrons) in high density phase will feel more weaker attractive (repulsive) effects from nuclear symmetry potentials. Therefore, with a certain L but varying

¹ Approximately at $t = 13$ fm/c, the reaction approaches maximum compression, the nucleons in compression region are naturally in dense but low energy phase.

² The value of 81 MeV is the transition kinetic energy for the nuclear symmetry potential at $1.5\rho_0$ with $L = 62.7$ MeV and $U_{sym}^\infty(\rho_0) = -240$ MeV.

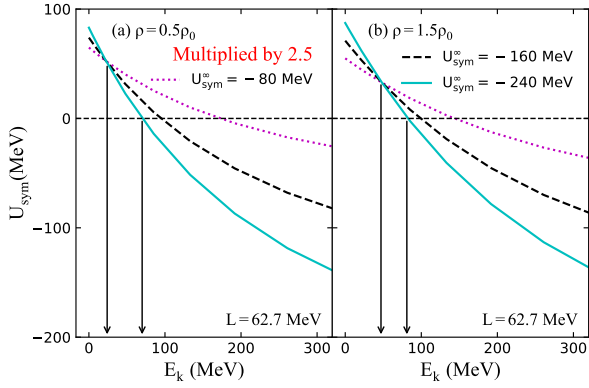


FIG. 8. (Color online) Momentum/kinetic-energy dependent nuclear symmetry potential at $\rho = 0.5\rho_0$ (a) and $\rho = 1.5\rho_0$ (b) with different $U_{sym}^\infty(\rho_0)$ calculated from the IMDI interaction. The values of nuclear symmetry potential at $\rho = 0.5\rho_0$ are multiplied by a factor of 2.5.

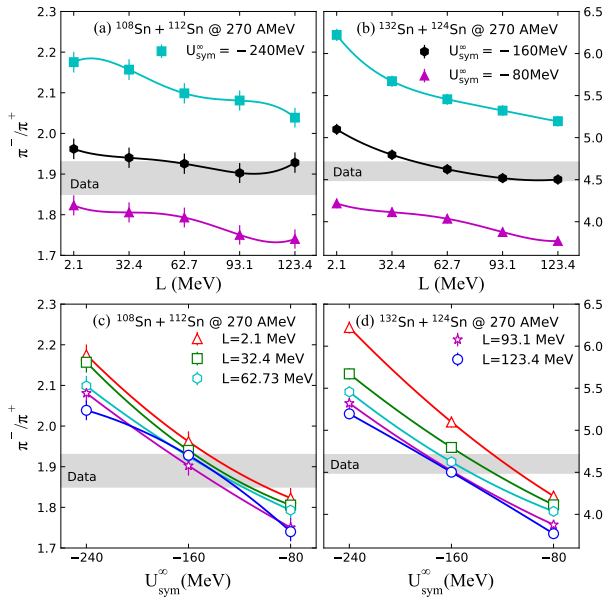


FIG. 9. (Color online) Upper: Ratios of π^-/π^+ generated in reactions $^{108}\text{Sn} + ^{112}\text{Sn}$ (a) and $^{132}\text{Sn} + ^{124}\text{Sn}$ (b) with different $U_{sym}^\infty(\rho_0)$ as a function of the L in comparison with the corresponding S π RIT data; Lower: Ratios of π^-/π^+ generated in reactions $^{108}\text{Sn} + ^{112}\text{Sn}$ (c) and $^{132}\text{Sn} + ^{124}\text{Sn}$ (d) with different L as a function of the $U_{sym}^\infty(\rho_0)$ in comparison with the corresponding S π RIT data.

the $U_{sym}^\infty(\rho_0)$ from -80 to -240 MeV, the repulsive scalar potential and the *weakened attractive* nuclear symmetry potential can cause some protons to increase their kinetic energies up to 150 MeV and above. It should be emphasized that for the reaction with a certain $U_{sym}^\infty(\rho_0)$ one usually can interpret the effects of L on pion production through the density criterion, i.e., average maximum densities formed in the reaction compressed stages.

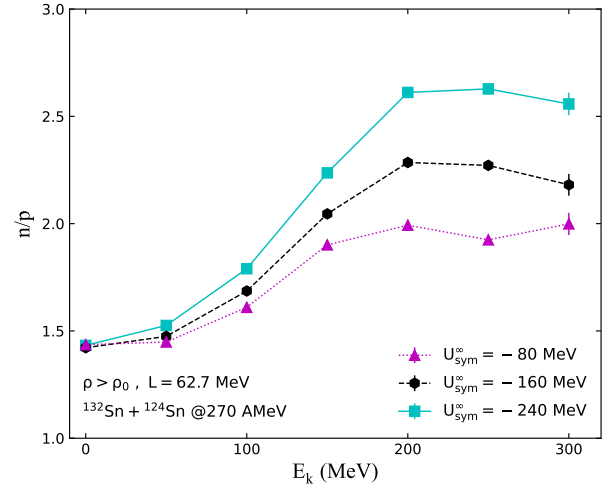


FIG. 10. (Color online) Kinetic energy distribution of neutrons over protons n/p with local densities higher than ρ_0 produced at $t = 20$ fm/c in the reaction $^{132}\text{Sn} + ^{124}\text{Sn}$ with different $U_{sym}^\infty(\rho_0)$ and a certain L .

Nevertheless, for the case with a certain L , interpreting the effects of $U_{sym}^\infty(\rho_0)$ on pion production needs both density and energy criterions because a small reduction of the average maximum densities formed in the reaction compressed stages but a significant increase of the kinetic energy for these high density nucleons could also lead to increased production of pions.

Shown in Fig. 9 are the π^-/π^+ ratios of theoretical simulations for the same reactions in comparison with the S π RIT data. First, consistent with the observations of most transport models, it is seen from the upper windows of Fig. 9 that the π^-/π^+ ratios indeed are more sensitive to the L compared to the pion yields, and a softer nuclear symmetry energy with a smaller L value leads to a higher π^-/π^+ ratio. Moreover, for the more neutron-rich reaction $^{132}\text{Sn} + ^{124}\text{Sn}$, the π^-/π^+ ratios show more sensitivities to the L . Second, it is seen from the lower windows of Fig. 9 that with a certain L value the π^-/π^+ ratios are increasing with the value of $|U_{sym}^\infty(\rho_0)|$. Actually, similar as that for more pion production, this observation can also be understood by examining the kinetic energy distribution of neutrons over protons n/p with local densities higher than ρ_0 at $t = 20$ fm/c in reactions $^{132}\text{Sn} + ^{124}\text{Sn}$ with a certain L as shown in Fig. 10. It is seen that with a certain $L = 62.7$ MeV the ratio n/p is increasing with varying the $U_{sym}^\infty(\rho_0)$ from -80 to -240 MeV, due to the increment of high energy neutrons is larger than that of protons for the neutron-rich reactions. This is the reason we can observe that with a certain L value the π^-/π^+ ratios are increasing with the value of $|U_{sym}^\infty(\rho_0)|$ as shown in Fig. 9. In addition, compared with the S π RIT data, our results on π^-/π^+ ratios also fit quite well the experimental data within a certain range for the value of $U_{sym}^\infty(\rho_0)$.

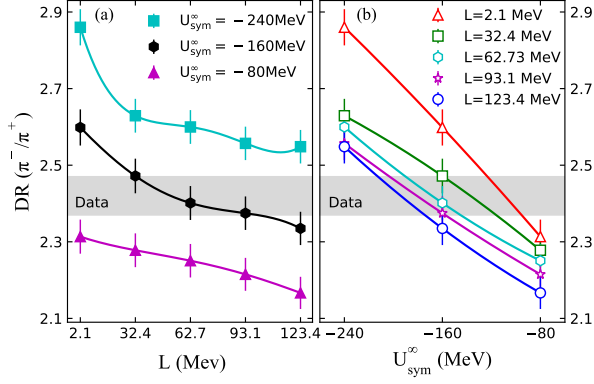


FIG. 11. (Color online) The double π^-/π^+ ratios [i.e., $DR(\pi^-/\pi^+)$] of the reactions $^{132}\text{Sn} + ^{124}\text{Sn}$ over $^{108}\text{Sn} + ^{112}\text{Sn}$ with different $U_{sym}^\infty(\rho_0)$ as a function of the L (a) and different L as a function of the $U_{sym}^\infty(\rho_0)$ (b) in comparison with the corresponding S π RIT data.

As a more clean observable, the double ratio of two reactions, i.e., $DR(\pi^-/\pi^+)$ ratio of reactions $^{132}\text{Sn} + ^{124}\text{Sn}$ over $^{108}\text{Sn} + ^{112}\text{Sn}$, has the advantages of reducing both the isoscalar potential effects and the Coulomb field effects, and thus is expected to disentangle the effects of nuclear symmetry potential/energy from those of both isoscalar potentials and Coulomb fields in HICs. Therefore, we show in Fig. 11 the $DR(\pi^-/\pi^+)$ ratios of two reactions in comparison with the S π RIT data. It is seen from the left panel of Fig. 11 that the $DR(\pi^-/\pi^+)$ ratios of two reactions indeed are more sensitive to the high density nuclear symmetry energy. Moreover, the $DR(\pi^-/\pi^+)$ ratios are also more clearly separated by varying the value of $U_{sym}^\infty(\rho_0)$ from -80 to -240 MeV, and thus more sensitive to the momentum dependence of nuclear symmetry potential as indicated in the right panel of Fig. 11.

Now, we use above three observables, i.e., pion yields and their single π^-/π^+ as well as double $DR(\pi^-/\pi^+)$ ratios, to constrain the value of $U_{sym}^\infty(\rho_0)$. To this end, we perform the systematic error analyses for pion yields as well as their single π^-/π^+ and double $DR(\pi^-/\pi^+)$ ratios at different $U_{sym}^\infty(\rho_0)$. Apart from the pion yields as well as their single π^-/π^+ and double $DR(\pi^-/\pi^+)$ ratios at $U_{sym}^\infty(\rho_0) = -80, -160$ and -240 MeV, the values of these observables at other $U_{sym}^\infty(\rho_0)$ with an interval of 10 MeV are obtained by interpolating the simulation ones. Shown in Fig. 12 are contours of the relative error as a two dimensional function of L and $U_{sym}^\infty(\rho_0)$. Unfortunately, it seems hard to constrain the value of L from the relative errors between theoretical simulations and experimental data before determining the characteristic parameter $U_{sym}^\infty(\rho_0)$ of nuclear symmetry potential. Nevertheless, it is obvious to see that we still have the opportunities to constrain the $U_{sym}^\infty(\rho_0)$ into a certain range. Therefore, to extract relative accurate constraints on $U_{sym}^\infty(\rho_0)$, we limit the values of L in the range from

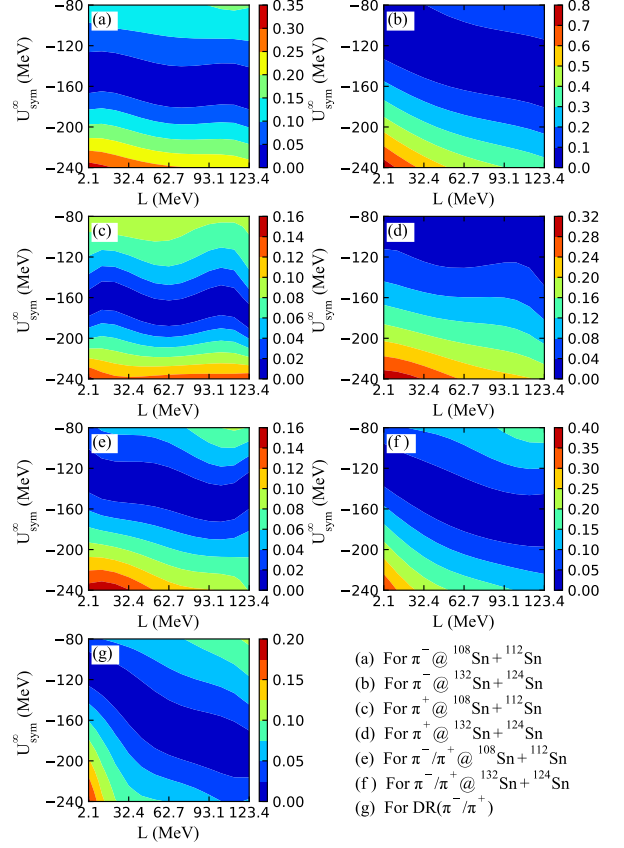


FIG. 12. (Color online) Contours of the relative errors for pion yields as well as their single and double pion ratios as a function of L and U_{sym}^∞ in reactions $^{108}\text{Sn} + ^{112}\text{Sn}$ and $^{132}\text{Sn} + ^{124}\text{Sn}$.

32.4 to 123.4 MeV since this range for L basically covers the possible range for L extracted from the existing literatures in experiments and/or theories [5, 10, 60–68]. Shown in Fig. 13 are the relative error of pion observables between theoretical simulations and corresponding data in S π RIT experiments.³ First, we use the π^-/π^+ and double $DR(\pi^-/\pi^+)$ ratios to constrain the $U_{sym}^\infty(\rho_0)$ since the pion ratios are relative clean than pion yields. It is seen that to ensure the errors between theoretical simulations of both π^-/π^+ and double $DR(\pi^-/\pi^+)$ ratios and corresponding data in S π RIT experiments to be within 4% that is the maximum uncertainties of experimental data, the value of $U_{sym}^\infty(\rho_0)$ should be constrained between -163.5 and -156 MeV as indicated by the arrows in Fig. 13. Moreover, If considering to use both π^- and π^+ to further constrain the $U_{sym}^\infty(\rho_0)$, the value of $U_{sym}^\infty(\rho_0) = -156.5 \pm 0.5$ MeV is favored to ensure the errors of both pion yields and pion ratios between theoretical simulations and corresponding data to be within 4%.

³ In Fig. 13, the simulation results with $L = 2.1$ MeV have been removed in interpolating pion observables for other $U_{sym}^\infty(\rho_0)$.

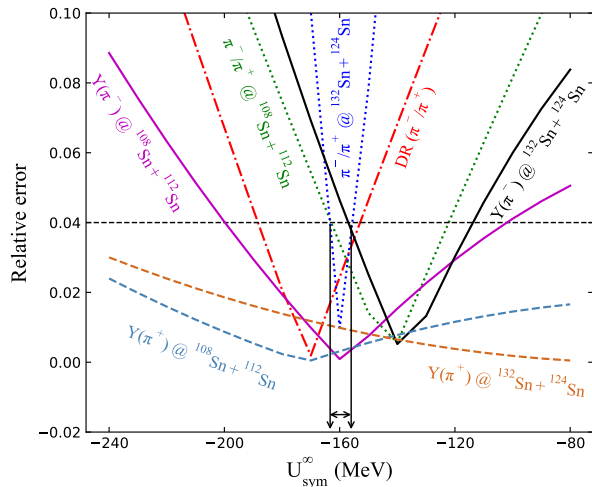


FIG. 13. (Color online) Relative errors for the pion yields as well as their single and double pion ratios as a function the U_{sym}^{∞} in reactions $^{108}\text{Sn} + ^{112}\text{Sn}$ and $^{132}\text{Sn} + ^{124}\text{Sn}$.

On the other hand, it is well known that the isospin splitting of in-medium nucleon effective mass is resulting from the momentum dependence of nuclear symmetry potential. Therefore, it is necessary to use our constrained $U_{sym}^{\infty}(\rho_0)$, i.e., $-163.5 \leq U_{sym}^{\infty}(\rho_0) \leq -156$ MeV, to evaluate the isospin splitting of in-medium nucleon effective mass. According to the formula of nucleon effective mass, i.e.,

$$m_{\tau}^*/m = \left[1 + \frac{m}{k_{\tau}} \frac{dU_{\tau}}{dk}\right]^{-1}, \quad (9)$$

the neutron-proton effective mass splitting Δm_{np}^* for the reaction $^{132}\text{Sn} + ^{124}\text{Sn}$ is constrained between 0.1335 and 0.1384 MeV. Moreover, if the value of $U_{sym}^{\infty}(\rho_0) = -156.5 \pm 0.5$ MeV is used, the corresponding Δm_{np}^* for the reaction $^{132}\text{Sn} + ^{124}\text{Sn}$ is constrained between 0.1335 and 0.1342 MeV.

Before ending this part, we give a useful remark here. Presently, since we do not know the exact information of L , it is therefore we have considered all possible range for

L during conducting the error analyses to constrain the $U_{sym}^{\infty}(\rho_0)$. Undoubtedly, stringent constraints on L from both experiments and theories in future could improve this constraint on $U_{sym}^{\infty}(\rho_0)$.

IV. SUMMARY

In conclusion, we have studied effects of the momentum dependent characteristic parameter $U_{sym}^{\infty}(\rho_0)$ of nuclear symmetry potential on pion production in central Sn + Sn collisions at 270 MeV/nucleon. It is found that with a certain L value the characteristic parameter $U_{sym}^{\infty}(\rho_0)$ of nuclear symmetry potential also affects the production of π^- and π^+ as well as their pion ratios. This naturally provides the opportunity to constrain the value of $U_{sym}^{\infty}(\rho_0)$ through comparing the pion observable of theoretical simulations with the corresponding data in HICs. Therefore, through conducting the systematic error analyses for pion observables of reactions $^{108}\text{Sn} + ^{112}\text{Sn}$ and $^{132}\text{Sn} + ^{124}\text{Sn}$, we find that the value of $U_{sym}^{\infty}(\rho_0)$ can be constrained between -163.5 and -156 MeV that can ensure the errors between theoretical simulations of both π^-/π^+ and double DR(π^-/π^+) ratios and corresponding data in π RIT experiments to be within 4%. If considering to use both π^- and π^+ to further constrain the $U_{sym}^{\infty}(\rho_0)$, the value of $U_{sym}^{\infty}(\rho_0) = -156.5 \pm 0.5$ MeV is favored to ensure the errors of both pion yields and pion ratios between theoretical simulations and corresponding data to be within 4%. Moreover, considering that the isospin splitting of in-medium nucleon effective mass is resulting from the momentum dependence of nuclear symmetry potential, we have also discussed the neutron-proton effective mass splitting.

ACKNOWLEDGMENTS

G.F.W. would like to thank Profs. B. A. Li and G. C. Yong for helpful discussions. This work is supported by the National Natural Science Foundation of China under grant Nos.11965008, 11405128, and Guizhou Provincial Science and Technology Foundation under Grant No.[2020]1Y034, and the PhD-funded project of Guizhou Normal university (Grant No.GZNU[2018]11).

- [1] S. Typel, and B. A. Brown, Phys. Rev. C **64**, 027302 (2001).
- [2] E. E. Kolomeitsev, C. Hartnack, H. W. Barz, M. Bleicher, E. Bratkovskaya, W. Cassing, L. W. Chen, P. Danielewicz, C. Fuchs, T. Gaitanos, C. M. Ko, A. Larionov, M. Reiter, Gy. Wolf and J. Aichelin, J. Phys. G:Nucl. Part. Phys. **31**, S741 (2005).
- [3] V. Baran, M. Colonna, V. Greco and M. Di Toro, Phys. Rep. **410**, 335 (2005).

- [4] B.A. Li, L.W. Chen and C.M. Ko, Phys. Rep. **464**, 113 (2008).
- [5] A. Tamii, I. Poltoratska, P. von-Neumann-Cosel, Y. Fujita, T. Adachi, C. A. Bertulani, J. Carter, M. Dozono, H. Fujita, K. Fujita *et al.*, Phys. Rev. Lett. **107**, 062502 (2011).
- [6] X. Viñas, M. Centelles, X. Roca-Maza, and M. Warda, Eur. Phys. J. A **50**, 27 (2014)
- [7] C. J. Horowitz, E. F. Brown, Y. Kim, W. G. Lynch, R. Michaels, A. Ono, J. Piekarewicz, M. B. Tsang, and H. H.

- Wolter, J. Phys. G:Nucl. Part. Phys. **41**, 093001 (2014).
- [8] P. G. Reinhard, and W. Nazarewicz, Phys. Rev. C **93**, 051303 (2016).
- [9] M. Baldo, G. F. Burgio, Prog. Part. Nucl. Phys. **91**, 203 (2016).
- [10] J. Estee, W. G. Lynch, C. Y. Tsang, J. Barney, G. Jhang, M. B. Tsang, R. Wang, M. Kaneko *et al.* ($S\pi$ RIT Collaboration), and M. D. Cozma, Phys. Rev. Lett. **126**, 162701 (2021).
- [11] C. Y. Tsang, M. B. Tsang, P. Danielewicz, F. J. Fattoyev, and W. G. Lynch, Phys. Lett. B **796**, 1 (2019).
- [12] Y. Lim and J. W. Holt, Phys. Rev. Lett. **121**, 062701 (2018).
- [13] I. Tews, J. Margueron, and S. Reddy, Phys. Rev. C **98**, 045804 (2018).
- [14] A. Drago, A. Lavagno, G. Pagliara, and D. Pigato, Phys. Rev. C **90**, 065809 (2014).
- [15] A. W. Steiner, and S. Gandolfi, Phys. Rev. Lett. **108**, 081102 (2012).
- [16] C. Ducoin, J. Margueron, C. Providência, and I. Vidaña, Phys. Rev. C **83**, 045810 (2011).
- [17] J. M. Lattimer, and M. Prakash, Phys. Rep. **621**, 127 (2016).
- [18] B. A. Brown, Phys. Rev. Lett. **111**, 232502 (2013).
- [19] P. Danielewicz, R. Lacey, and W. G. Lynch, Science **298**, 1592 (2002).
- [20] M. Oertel, M. Hempel, T. Klähn, and S. Typel, Rev. Mod. Phys. **89**, 015007 (2017).
- [21] G. W. Hoffmann, and W. R. Coker, Phys. Rev. Lett. **29**, 227 (1972).
- [22] A. J. Koning *et al.*, Nucl. Phys. A **713**, 231 (2003).
- [23] J. P. Jeukenne, C. Mahaux, and R. Sartor, Phys. Rev. C **43**, 2211 (1991).
- [24] G. Jhang, J. Estee, J. Barney, G. Cerizza, M. Kaneko, J. W. Lee, W. G. Lynch, T. Isobe *et al.* ($S\pi$ RIT Collaboration), M. Colonna, D. Cozma, P. Danielewicz, H. Elfner, N. Ikeno, C. M. Ko, J. Mohs, D. Oliinychenko *et al.* (TMEP Collaboration), Phys. Lett. B **813**, 136016 (2021).
- [25] R. Shane, A. B. McIntosh, T. Isobe, W. G. Lynch, H. Baba, J. Barney, Z. Chajceki, M. Chartier, *et al.*, Nuclear Instruments and Methods in Physics Research A **784**, 513 (2015).
- [26] W. Reisdorf *et al.* (FOPI Collaboration), Nucl. Phys. A **781**, 459 (2007); Nucl. Phys. A **848**, 366 (2010); Nucl. Phys. A **876**, 1 (2012).
- [27] G. C. Yong, Phys. Rev. C **104**, 014613 (2021).
- [28] R. Subedi, R. Shneor, P. Monaghan, B. D. Anderson, K. Aniol, J. Annand, J. Arrington and H. Benaoum *et al.*, Science **320**, 1476 (2008).
- [29] L. B. Weinstein, E. Piasezky, D. W. Higinbotham, J. Gomez, O. Hen, and R. Shneor, Phys. Rev. Lett. **106**, 052301 (2011).
- [30] M. M. Sargsian, Phys. Rev. C **89**, 034305 (2014).
- [31] C. Ciofi degli Atti, Phys. Rep. **590**, 1 (2015).
- [32] O. Hen, M. Sargsian, L. B. Weinstein, E. Piasezky, H. Hakobyan *et al.*, Science **346**, 614 (2014).
- [33] M. Duer, O. Hen, E. Piasezky, H. Hakobyan, L. B. Weinstein, M. Braverman, E. O. Cohen, D. Higinbotham *et al.* (CLAS Collaboration), Nature **560**, 617 (2018).
- [34] K. A. Brueckner, J. Dabrowski, Phys. Rev. **134**, B722 (1964).
- [35] J. Dabrowski, P. Haensel, Phys. Rev. C **7**, 916 (1973).
- [36] J. Dabrowski, P. Haensel, Can. J. Phys. **52**, 1768 (1974).
- [37] V. Giordano, M. Colonna, M. D. Toro, V. Greco, and J. Rizzo, Phys. Rev. C **81**, 044611 (2010).
- [38] C. B. Das, S. Das Gupta, C. Gale, and B. A. Li, Phys. Rev. C **67**, 034611 (2003).
- [39] B. A. Li, C. B. Das, S. Das Gupta, and C. Gale, Phys. Rev. C **69**, 011603(R) (2004).
- [40] L. W. Chen, B. A. Li, A note of an improved MDI interaction for transport model simulations of heavy ion collisions (Unpublished, Texas A&M University-Commerce, 2010).
- [41] C. Xu, B. A. Li, Phys. Rev. C **81**, 044603 (2010).
- [42] L. W. Chen, C. M. Ko, B. A. Li, C. Xu, and J. Xu, Eur. Phys. J. A **50**, 29 (2014).
- [43] G. F. Wei, C. Xu, W. Xie, Q. J. Zhi, S. G. Chen, and Z. W. Long, Phys. Rev. C **102**, 024614 (2020).
- [44] J. Dechargé, D. Gogny, Phys. Rev. C **21**, 1568 (1980).
- [45] J. Xu, L. W. Chen, and B. A. Li, Phys. Rev. C **91**, 014611 (2015).
- [46] H. Y. Kong, J. Xu, L. W. Chen, B. A. Li, and Y. G. Ma, Phys. Rev. C **95**, 034324 (2017).
- [47] S. Hama, B. C. Clark, E. D. Cooper, H. S. Sherif, and R. L. Mercer, Phys. Rev. C **41**, 2737 (1990).
- [48] O. Buss, T. Gaitanos, K. Gallmeister, H. van Hees, M. Kaskulov, O. Lalakulich, A. B. Larionov, T. Leitner, J. Weil, and U. Mosel, Phys. Rep. **512**, 1 (2012).
- [49] M. Ericson, T. E. O. Ericson, Ann. of Phys. **36**, 323 (1966).
- [50] C. García-Recio, E. Oset, and L. L. Salcedo, Phys. Rev. C **37**, 194 (1988).
- [51] J. Nieves, E. Oset, and C. García-Recio, Nucl. Phys. A **554**, 554 (1993).
- [52] G. F. Wei, C. Liu, X. W. Cao, Q. J. Zhi, W. J. Xiao, C. Y. Long, and Z. W. Long, Phys. Rev. C **103**, 054607 (2021).
- [53] J. Xu, L. W. Chen, C. M. Ko, B. A. Li, and Y. G. Ma, Phys. Rev. C **87**, 067601 (2013).
- [54] J. Hong, P. Danielewicz, Phys. Rev. C **90**, 024605 (2014).
- [55] T. Song, C. M. Ko, Phys. Rev. C **91**, 014901 (2015).
- [56] Z. Zhang, and C. M. Ko, Phys. Rev. C **95**, 064604 (2017).
- [57] G. F. Wei, B. A. Li, G. C. Yong, L. Ou, X. W. Cao, and X. Y. Liu, Phys. Rev. C **97**, 034620 (2018).
- [58] G. F. Wei, G. C. Yong, L. Ou, Q. J. Zhi, Z. W. Long, and X. H. Zhou, Phys. Rev. C **98**, 024618 (2018).
- [59] B. A. Li, G. C. Yong, and W. Zuo, Phys. Rev. C **71**, 014608 (2005).
- [60] J. M. Lattimer, and Y. Lim, Astrophys. J. **771**, 51 (2013).
- [61] X. Roca-Maza, X. Viñas, M. Centelles, B. K. Agrawal, G. Colò, N. Paar, J. Piekarewicz, and D. Vretenar, Phys. Rev. C **92**, 064304 (2015).
- [62] P. Russotto, S. Gannon, S. Kupny, P. Lasko, L. Acosta, M. Adamczyk, A. Al-Ajlan, M. Al-Garawi *et al.*, Phys. Rev. C **94**, 034608 (2016).
- [63] K. Hebeler, J. M. Lattimer, C. J. Pethick, and A. Schwenk, Phys. Rev. Lett. **105**, 161102 (2010).
- [64] I. Tews, T. Krüger, K. Hebeler, and A. Schwenk, Phys. Rev. Lett. **110**, 032504 (2013).
- [65] D. Lonardonì, I. Tews, S. Gandolfi, and J. Carlson, Phys. Rev. Res. **2**, 022033 (2020).
- [66] C. Drischler, R. J. Furnstahl, J. A. Melendez, and D. R. Phillips, Phys. Rev. Lett. **125**, 202702 (2020).
- [67] B. T. Reed, F. J. Fattoyev, C. J. Horowitz, and J. Piekarewicz, Phys. Rev. Lett. **126**, 172503 (2021).

- [68] R. Essick, I. Tews, P. Landry, and A. Schwenk, Phys. Rev. Lett. **127**, 192701 (2021) and references therein.